Title

On producing CO2 from subsurface reservoirs: simulations of liquid-gas phase change caused by decompression

Journal

Greenhouse Gases Science and Technology, 9(2)

ISSN

2152-3878

Authors

Oldenburg, Curtis
Pan, Lehua
Zhou, Quanlin
et al.

Publication Date

2019-04-01

DOI

10.1002/ghg.1852

Peer reviewed

On Producing CO_2 from Subsurface Reservoirs:

Simulations of Liquid-Gas Phase Change Caused by Decompression

C.M. Oldenburg[1], L. Pan[1], Q. Zhou[1], L. Dobeck[2], and L. Spangler[2]

[1]Energy Geosciences Division

Lawrence Berkeley National Laboratory

Berkeley, CA 94720

[2]Energy Research Institute

Montana State University

Bozeman, MT 59717

January 3, 2019

Keywords: Natural CO2 reservoir, Kevin Dome, CO_2 withdrawal, TOUGH, ECO2N, CO_2 phase change, Joule Thompson cooling

Abstract

Carbon dioxide (CO_2) extraction from deep reservoirs is currently important in CO_2-EOR (enhanced oil recovery) and may become important in the future if interim CO_2 storage becomes common. In late 2014, we were involved in a production test of liquid CO_2 from the Middle Duperow dolostone at Kevin Dome, Montana. The test resulted in lowering the temperature at the well bottom to ~2 ºC, and showed that the well and reservoir have very low CO_2 productivity. We have used the CO_2 modeling capabilities of the TOUGH codes to simulate the test and show that liquid CO_2 in the reservoir changes to gas phase as the pressure is lowered in the well during production testing. The associated phase change and decompression combine to drastically lower bottom-hole temperature creating the potential for water ice or CO_2 hydrate to form. By hypothesizing a relatively high-permeability damage zone near the well surrounded by lower-permeability reservoir rock, we can match the observed pressure, temperature, and production rate. Moving from the Kevin Dome test to the question of CO_2 extraction from deep reservoirs in general, we carried out a parametric study to investigate the effects of reservoir depth and transmissivity on CO_2 production rate for a prototypical reservoir. Simulations show that large depth and high transmissivity favor productivity. Complex phase changes within the ranges of *P-T* encountered in typical CO_2 production wells affect production rates. The results of our parametric study may be useful for preliminary feasibility assessment of CO_2 extraction from deep reservoirs.

Introduction

Carbon dioxide (CO_2) extraction from subsurface reservoirs using deep wells is an essential process in current large-scale utilization of CO_2. For example, CO_2 is needed for CO_2-EOR (enhanced oil recovery), and this CO_2 is mostly sourced from natural CO_2 accumulations in deep subsurface reservoirs. If the CO_2 is being recovered from a natural accumulation or dome, the extraction process is usually referred to as "production," whereas if the CO_2 is being extracted from a secondary or interim storage reservoir, it is usually called "withdrawal." As normally envisioned, CO_2 stored in interim reservoirs will be anthropogenic CO_2[1], although it could also be natural CO_2. While such interim storage reservoirs for anthropogenic CO_2 may be common in the future, the main activity today involves production from natural CO_2 reservoirs for CO_2-EOR and these include Sheep Mountain and McElmo Domes in Colorado, Bravo Dome, New Mexico, and Farnham Dome, Utah, Springerville, Arizona, and Big Piney-LaBarge, Wyoming[2]. Another significant dome under production is Jackson Dome, Mississippi[3]. The Quebrache CO_2 reservoir in Mexico has also been suggested as a viable natural source of CO_2 [4, 5].

The production or withdrawal of CO_2 from deep wells is complicated by the fact that CO_2 has phase-change boundaries that coincidentally straddle natural pressure-temperature (*P-T*) ranges typical of wells accessing most oil, gas, and CO_2 resources. This can be seen in Figure 1 by the crossing of phase boundaries of the two *P-T* paths shown by the heavy dashed lines corresponding to 15 ºC/km and 30 ºC/km geothermal gradients. If the temperature gradient is a

little smaller than average, CO_2 can be in liquid conditions in the subsurface. As for CO_2 moving upward in a well, it may follow a *P-T* path causing it to change phase during upward flow from supercritical to gaseous phases in the case of high geothermal gradient. In the case of low geothermal gradient, CO_2 phase may change from supercritical to liquid to gaseous when the production rate is small and the temperature of well CO_2 follows the thermal gradient, or from supercritical to gaseous for high-rate production without thermal equilibrium. In most cases an aqueous phase will also be present resulting in more complicated multiphase flow in the well and/or in the reservoir.

In general, during the production or withdrawal of CO_2 from a well, hereafter referred to as production, the pressure must be lower in the well than in the reservoir. Therefore CO_2 expands as it moves from the reservoir into the well and for CO_2 or CO_2 with impurities this expansion causes cooling[6,7]. In addition, if the CO_2 is initially in liquid conditions, as pressure is lowered the CO_2 will change phase to gas and expand, with absorption of the latent heat of vaporization from surrounding rock and fluids causing further (more significant) cooling. In short, phase change and expansion of CO_2 associated with production of CO_2 can lead to large temperature drops. In the deep subsurface, water is ubiquitous and therefore ice and/or CO_2 hydrate phases can form if the cooling is large enough to bring *P-T* conditions into ice or hydrate stability regions. This is particularly true when the interface of liquid and gaseous CO_2 remains stable in the reservoir level and continuous cooling eventually forms hydrates near the wellbore-reservoir region.

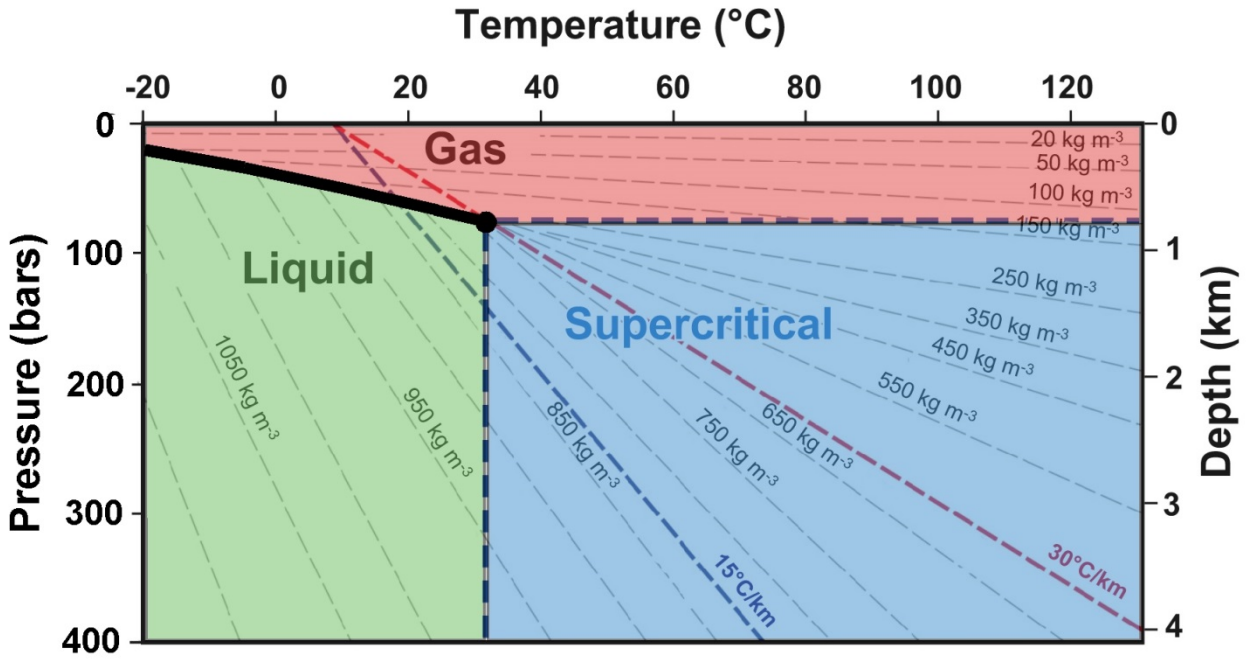

Figure 1. Stylized CO_2 phase diagram with gas, liquid, and supercritical regions colored and superimposed on isopleths of density and two P-T paths showing that depending on the geothermal gradient, which typically ranges from 15 ºC/km to 30 ºC/km as shown by the heavy blue and red dashed lines, CO_2 can be in supercritical, liquid, or gaseous conditions at different depths in the subsurface or in a well (after Oldenburg[8]).

In 2014, the Big Sky Carbon Sequestration Partnership (BSCSP) conducted a production test of liquid CO_2 from a large natural CO_2 reservoir in the Duperow dolostone at Kevin Dome, Montana. The Danielson 33-17 well was tested repeatedly over several days and showed effects of extreme cooling and phase change and consistently low CO_2 production rate. Successful CO_2 production (and injection) is dependent on both an effective flow conduit being provided by the well, but also effective permeability (or permeability-thickness product, i.e., transmissivity) in the reservoir. Severe cooling processes caused by expansion and phase change have the potential to cause hydrate and/or water ice formation that can affect CO_2 flow in the well and/or in the reservoir.

The purpose of the first part of this paper is to present simulations and analysis of the 2014 Danielson 33-17 CO_2 production test at Kevin Dome, Montana. We show that effective permeability variation in the near-well region can explain the observed *P-T* response during the test. In the second part of the paper, we expand on the successful modeling of the production test by carrying out a parametric study to examine some general conditions needed for efficient CO_2 production from subsurface reservoirs under a variety of conditions of pressure, temperature, and

permeability to map out the parameter space under which CO_2 production is technically feasible. The main purpose of the second part of the paper is to present information that informs how operators can efficiently produce (or withdraw) CO_2 for large-scale utilization, whether it is from reservoirs with natural accumulations or from interim storage reservoirs.

Background and Prior Work

Carbon dioxide has been produced from natural CO_2 accumulations (domes) for enhanced oil recovery (CO_2-EOR) since the early 1970's[9]. The urgent need to decrease anthropogenic CO_2 emissions is motivating CO_2 capture and utilization, with CO_2-EOR as a major potential use for captured CO_2[10]. Because the capture supply rate is likely relatively constant from sources such as baseload fossil-fuel power plants, and utilization for EOR likely will have variable demand over various time scales, there arises the need for large-scale subsurface interim storage[1]. Therefore, whether from natural accumulations or from interim storage reservoirs, it is necessary to understand the controls on the production of CO_2 from subsurface reservoirs.

Renfro[11] presented design concepts for the Sheep Mountain CO_2 production facilities in Colorado. Based on the bottom-hole *P-T* and depth conditions at Sheep Mountain and the CO_2 enthalpy-temperature phase diagram, he determined the phase compositions (fractions of liquid and gaseous CO_2) that would be obtained during production up the well from a "good" and "bad" well, where these were defined as wells with most of the pressure drop occurring in the well and in the reservoir, respectively. A few years after Renfro's study[11], a CO_2 well at the Sheep Mountain facility suffered a breach blowout resulting in rapid cooling causing the formation of dry ice cobbles that were erupted out of the ground[12].

Weeter and Halstead[13] used the same enthalpy-temperature relations as used by Renfro[11] to investigate phase compositions during production of CO_2 from McElmo Dome, Colorado. Both of these early studies recognized the complex phase conditions and potential phase transitions that occur when CO_2 from the reservoir at supercritical conditions is depressurized during production and transport up the well. Specifically, supercritical CO_2 along with water (aqueous phase) in the reservoir can either become a two-phase (CO_2 gas-aqueous) fluid mixture during transport as pressure drops, or it can become a three-phase (CO_2 gas-CO_2 liquid-aqueous) mixture depending on how low *P-T* become during decompression and/or phase change. Jokhio et al.[14] analyzed the effects on decline curve estimates of various gases (CO_2, N_2, H_2S) considered as contaminants for natural gas (methane) wells. None of these early studies considered flow from the reservoir explicitly aside from the mention of heating and resistance (pressure drop) provided by the rock (porous media flow and/or fracture-matrix interactions) in the reservoir.

A CO_2 production test from Kevin Dome, Montana was carried out in December of 2014 as part of the Big Sky Carbon Sequestration Partnership[15]. The Kevin Dome CO_2 reservoir was chosen to provide a source of CO_2 for the BSCSP's study of CO_2 injection for storage in the water leg of

the same structure[16,17]. The results of the production test showed very low production rates, and very low temperatures (T ~ º2 C) in the bottom-hole region. The difficulty of producing CO_2 along with low total dissolved solids (TDS) in the proposed water-leg storage zone caused the project to pivot from being a CO_2 production and injection test to being an overall evaluation of CO_2 storage potential in the region. These characterization studies are based on regional geological interpretations complemented by seismic data, laboratory studies of core, and numerical reservoir simulation studies. As part of this modified scope, we report here on our work simulating the 2014 production test at Kevin Dome and investigating the non-isothermal processes of CO_2 production in general that make producing CO_2 from subsurface reservoirs so challenging.

Methods

The modeling and simulation presented here are carried out using the TOUGH codes, and in particular a research code formed by combining the best features of ECO2N[18] and ECO2M[19] to make a code capable of handling the phase change and low temperatures that can arise during CO_2 production involving gaseous, liquid, and supercritical phases of CO_2 along with saline water. Briefly, the new integrated CO_2 module uses a non-iterative calculation of specific enthalpy of dissolved CO_2 under single-phase aqueous conditions to improve convergence during the appearance or disappearance of non-aqueous phases, scaled gas saturation as a primary variable in three-phase conditions to remove correlation in changes in primary variables, and a saturation-weighted-average method to calculate the dissolved CO_2 mass fraction in the aqueous phase and its associated density and specific enthalpy in three-phase conditions to ensure a smooth transition of the properties of the dissolved CO_2 when one CO_2 phase disappears. This new CO_2 module will be released under the TOUGH3 framework[20] in the near future.

Danielson 33-17 well production test

The BSCSP carried out a production test in the Danielson 33-17 well from December 6, 2014 to January 7, 2015. Periods of flow (production) and shut-in were imposed to observe the behavior of the well. Here, we present simulations of the last production test during the period December 26-28, 2014 followed by a 10-day shut-in. This test was instrumented with two downhole *P*-*T* sensors and showed a large temperature drop associated with decompression and phase change in the region of the perforations (i.e., bottom hole relative to this particular test). During this production and shut-in period, bottom-hole and wellhead *P*-*T* were measured continuously along with wellhead flow rates. Temperature and pressure logging along the whole well were carried out right before and after this test period.

Figure 2 shows a sketch of the Danielson 33-17 well highlighting the Testing Zone 5 where the subject test was carried out. As shown, the test region is in the Middle Duperow, a low-permeability fractured dolostone. Two relatively high-permeability zones (Intervals 11 and 10)

are recognized and the well was perforated in these zones as shown in Figure 2. The depth of Testing Zone 5 is 3,208 to 3,336 ft (978 to 1017 m), and the ambient *P-T* conditions are 7.9 MPa and 26 ºC, which suggest CO_2 is naturally in the liquid phase in this interval. (This reservoir temperature implies an average geothermal gradient of 20 ºC/km assuming an average annual 6 ºC (43 ºF) ground temperature.) Pressure and temperature logging confirmed the transition of CO_2 in the well from gaseous conditions above 2,250 ft (686 m) to liquid conditions below as shown in Figure 3. Note that we infer from the hysteretic temperature log shown in Figure 3 that there is an inherent lag time in thermal equilibration of the gauge that causes the upward-moving logging run to show higher-than-actual temperatures and the downward-moving logging run to show lower-than-actual temperatures.

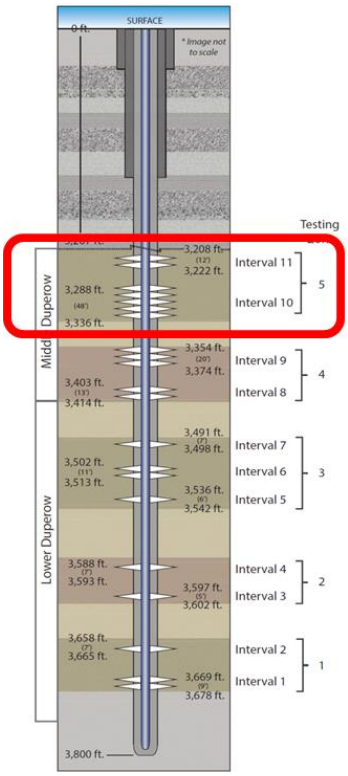

Figure 2. Diagram of the Danielson 33-17 well highlighting Testing Zone 5 in the Middle Duperow.

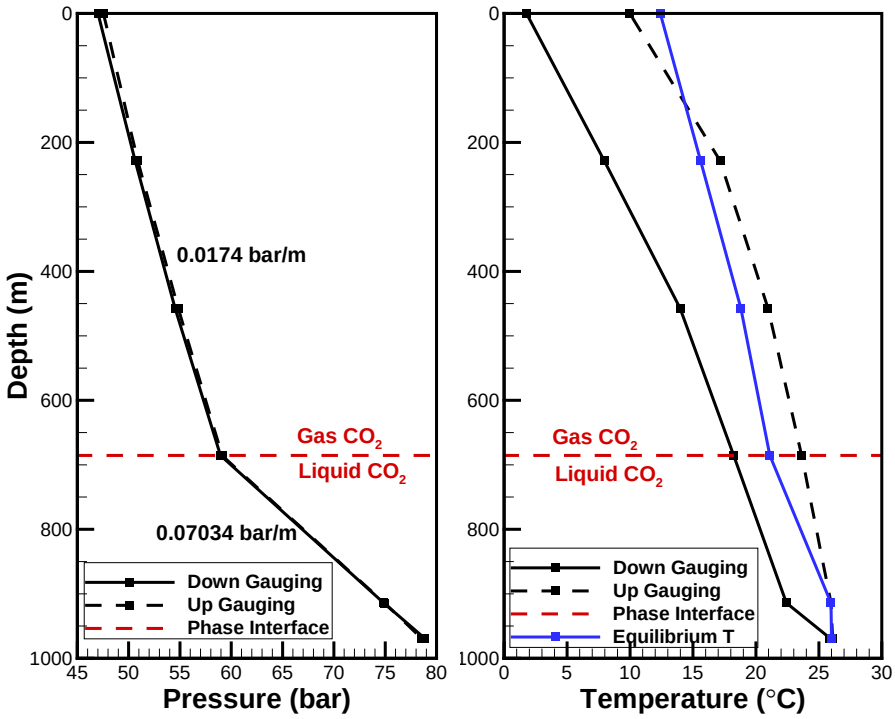

Figure 3. Profiles of pressure and temperature logged in the well. Logging by moving gauges down was carried out 12/26/14 and logging by moving the gauges up was carried out 1/7/15. Pressure rapidly equilibrates and the upward- and downward-gauging profiles match closely. For temperature, the instrument lags making upward-gauging show higher-than-actual temperatures and downward gauging show lower-than-actual temperatures. Note the distinctive gas-liquid transition apparent in the pressure profile.

We present in Figure 4 the main result of production testing in the Danielson 33-17 well carried out December 26-28, 2014. Shown in Figure 4 are pressure (red curve) and temperature (blue curve) at the bottom-hole (BH) gauge over time during the test which consisted of lowering the wellhead pressure to cause reservoir CO_2 to flow into the BH region of the well. Wellhead pressure was lowered in a controlled manner by opening a choke and venting CO_2 to the atmosphere at the rate of approximately 94 MSCFD (0.06 kg/s). Wellbore storage provides all of the mass of CO_2 vented during early time as the decompression wave moves down the well. After a time of approximately 1 hr, the BH pressure (BHP) was lowered from 7.9 MPa to 0.59 MPa resulting in a corresponding drop in temperature from 25.9 ºC to 2.2 ºC. This large temperature drop is most likely caused by expansion cooling and phase change of liquid CO_2 in the well to gaseous CO_2. As the CO_2 liquid flow to the well is restricted by the low permeability of the reservoir, less and less CO_2 is available to expand and flash to gas and the interface of liquid and gaseous CO_2 moves from the in situ depth (686 m) to the reservoir depth (~1,000 m), passing through the gauge depth at 969 m. This leads to formation ambient heat causing the slow

recovery of temperature as the test continues. After about 60 hours, the well was shut in and the pressure and temperature recovered to their ambient conditions.

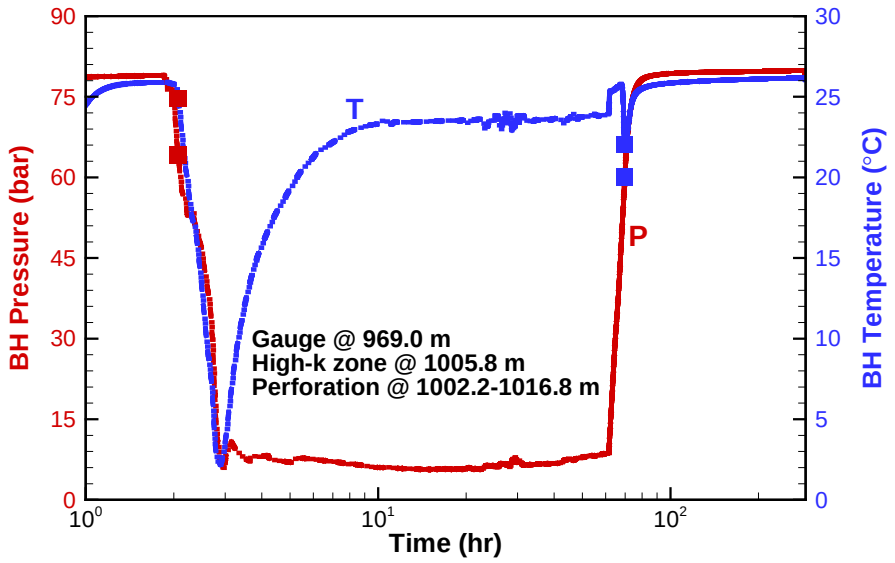

Figure 4. Bottom hole (BH) pressure (red) and temperature (blue) during the December 26-28, 2014 production test and the following shut-in test. As shown, production of CO_2 is accompanied by a rapid drop in temperature to approximately 2 ºC followed by a rising temperature as CO_2 flows from the reservoir to the well. The pressure rapidly recovers upon well shut-in following the test.

The flowrate of CO_2 peaked during the test at about 94 MSCFD (0.06 kg/s) at the beginning and stabilized after about 40 hours to around 40 MSCFD (0.026 kg/s) (1 MSCF = 28.3 m^3 × 1.98 kg/m^3 = 56.1 kg). These low flow rates were surprising at the time, but make sense if one considers that it is liquid CO_2 that must flow through the low-permeability Middle Duperow and the fractures and pore space may be filling up with hydrate as decompression and phase change occur causing temperatures well below the hydrate stability temperature for CO_2 at Middle Duperow depth.

TOUGH simulations of the production test

The low temperatures and phase-change processes observed in the well during the production test inspired thinking in the BSCSP project about how CO_2 production could be increased, and whether similar issues were important for CO_2 production more generally. Therefore we undertook modeling and simulation studies of CO_2 production starting with attempts to match the observations of the Danielson 33-17 production test as shown above.

We developed a radially symmetric *R-Z* grid as shown in Figure 5. The radial grid-block dimensions (*dR*) vary from 0.1 m near the well to 100 m at *R* = 1 km with perforations (aka perfs) at Intervals 11 and 10. The portion of the well below Resv3 is not included in the model because it was blocked-off during the test. Vertical resolution is variable with depth. For cap rock, it is about 1.67 m except for two top grid layers (corresponding to two sensors) where 0.3048 m is used. Each reservoir layer consists of one grid layer whose thicknesses are 4.26, 20.12, and 14.63 m, respectively. For the underlying layer, the grid layers are of uniform thickness of 2.97 m. The well is modeled as a high-*k* equivalent porous medium with zero capillary pressure and unit porosity with tubing of dimensions 2 7/8" (ID = 0.062 m) and casing 5 ½" (ID = 0.124 m). The low permeability and small fluid withdrawal justify using closed boundaries everywhere except for the top of the simulated well where either mass production rate or *P-T* conditions can be specified as time-varying boundary conditions. Note that the top of the simulated well is at a depth of 3,179 ft (968.96 m) rather than the ground surface. The reason for this choice is that (a) this was the location of a *P-T* gauge (Sensor #1) and (b) temperature in the well at shallower depths and particularly at the wellhead (exposed to the weather in December in Montana) would be below 0 ºC, which is the lower temperature limit of our CO_2 research simulator.

The properties of the permeable materials of the Middle Duperow (average core measurements) used in the model and for the well are shown in Table 1. In addition, thermal conductivity was assumed to be 2.50 W/m ^{o}C for Resv1-Resv4 and 4.50 W/m ^{o}C for everything else except for the annular region (from tube wall to casing wall) which has thermal conductivity of 25.1 W/m ^{o}C consistent with properties of steel casing.

A linear relative permeability function and no capillary pressure are used for the well whereas van Genuchten[21] relative permeability and capillary pressure functions (for aqueous phase) are used for the reservoir (Table 2). Corey's[22] relative permeability function is used for non-aqueous phases (gas and liquid CO_2) and the CO_2 liquid-phase capillary pressure is neglected.

Initial reservoir water saturation is 0.2 (lower than the residual saturation equal to 0.3) and the reservoir pressure is in equilibrium with the measured down hole well pressure. The cap rock is initially saturated with water under hydrostatic pressure. The initial water saturation in the well is assumed to be zero. The initial temperature varies with depth (derived from the wellbore upward and downward temperature log), resulting in temperature slightly higher than the 26 ^{o}C in the reservoir layers. The CO_2 is in liquid phase under the given reservoir *P-T* conditions. No salt is considered in these simulations.

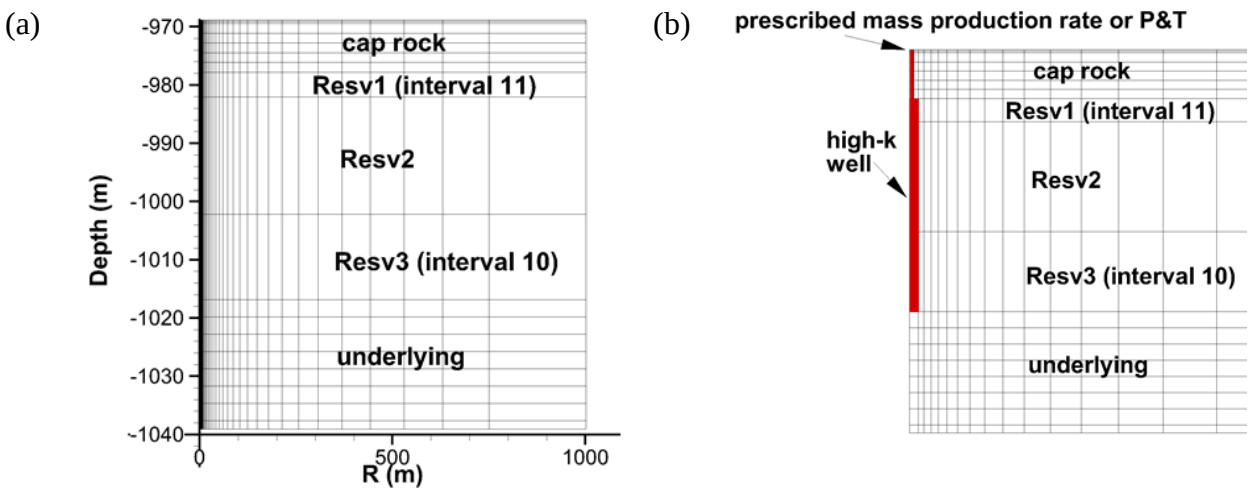

Figure 5. (a) Radially symmetric grid with relatively high-permeability intervals Resv1, Resv2 and Resv3 shown along with cap rock and underlying Duperow formation rock. (b) Close-up view of the near-well region showing the well which is modeled as a high-permeability feature.

Table 1. Properties of the Danielson 33-17 well production test model domain

Rock	Thickness (m)	Porosity	Horizontal k (10^{-18} m^2)	Vertical k (10^{-18} m^2)
Cap rock	8.99	0.03670	10.0	10.0
Resv1	4.27	0.0429	84.4	2.63
Resv2	20.12	0.0459	1.20	0.12
Resv3	14.63	0.0995	4090.0	2.35
underlying	23.77	0.9660	8.5	0.85
Well*	48.01	1.0	10^{10}	10^{10}

Table 2 Parameters of capillary pressure and relative permeability functions for all materials excluding the well

Parameter	Capillary pressure (Pa) vanGenuchten[21]	Aqueous phase Relative permeability (Pa) vanGenuchten[21]	Non-aqueous phase Relative permeability Corey[22]
Residual aqueous phase saturation	0.36	0.30	0.30
Saturated aqueous phase saturation	0.999	1.0	-
Residual non-aqueous phase saturation	-	-	0.20
Saturated non-aqueous phase saturation	-	-	1.00
λ (van Genuchten's m)	0.457	0.457	-
$1/P_0$ (Pa^{-1})	8.0×10^{-5}	-	-
Maximum capillary pressure (Pa)	1.0×10^{-6} for reservoir formations and 1.0×10^{-7} for others	-	-
Note	Capillary pressure of liquid CO_2 is assumed to be zero.		The non-aqueous phase relative permeability is then split into liquid and gas relative permeabilities proportional to their relative saturations.

As shown in Figure 5 by the label at the top of the model production well, in theory the production test can be simulated by specifying either the production rate or the *P-T* conditions at the top of the domain, i.e., at the well top. Note that the well top is the top of our model domain and is not the wellhead because we only modeled a short section of the well as shown in Figure 5. We present in Figure 6 simulation results using the permeability from Table 1 compared to production-test observations of pressure and temperature when we set the well-top boundary condition to the known mass production rate. As shown by the symbols, the pressure and temperature change only slightly when CO_2 is produced from the well at the known rate in contrast to the observed *P-T* which show large changes. Figure 6(b) shows the known production rate as specified at the top of the model well along with the measured rate. It is clear by the mismatch in *P-T* evolution that the model is missing some fundamental processes or properties controlling the behavior of the system.

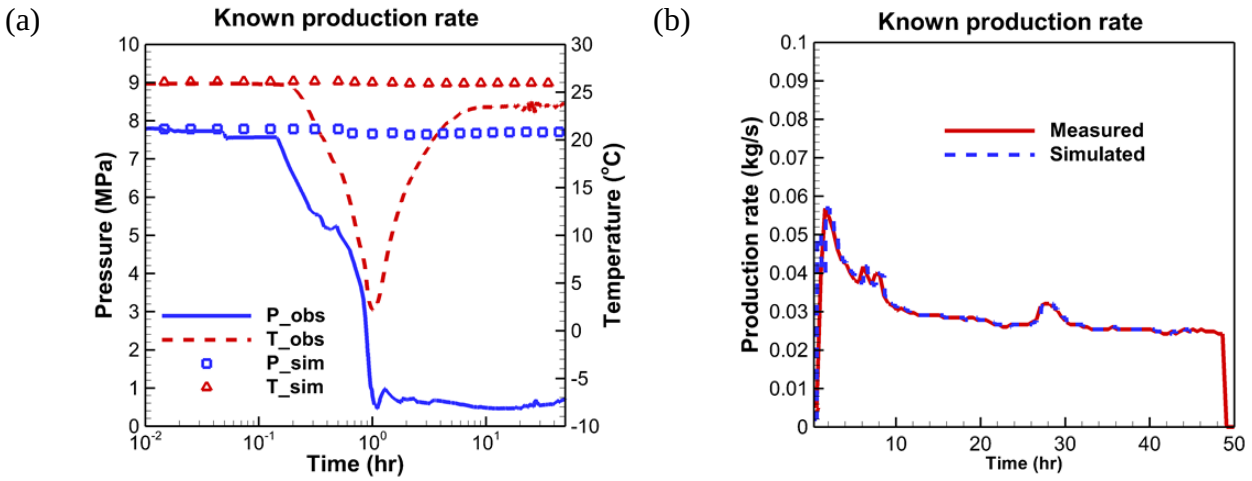

Figure 6. Results for specified mass production rate shown by (a) pressure and temperature variation over time during the production test as observed in the field experiment (lines) and in the model (symbols) at the lower gauge at depth = 3,180 ft (969.26 m) 1 ft from the well top with permeability as shown in Table 1, and by (b) measured and specified mass production rate at the top of the well and at 968.96 m, respectively.

We present in Figure 7 the simulated and measured results for the case of constant *P-T* at the top of the model well compared to the *P-T* at the downhole gauge at 3,180 ft (1 ft below the top of the model well). The simulated bottom-hole *P-T* satisfactorily matches observations early in the test, but after 1 hour the observed temperature strongly recovered whereas in the model system the temperature remains very low. Furthermore, the simulated production rate is much larger than the observed. Again, the model is clearly either missing essential physics or has incorrect system properties.

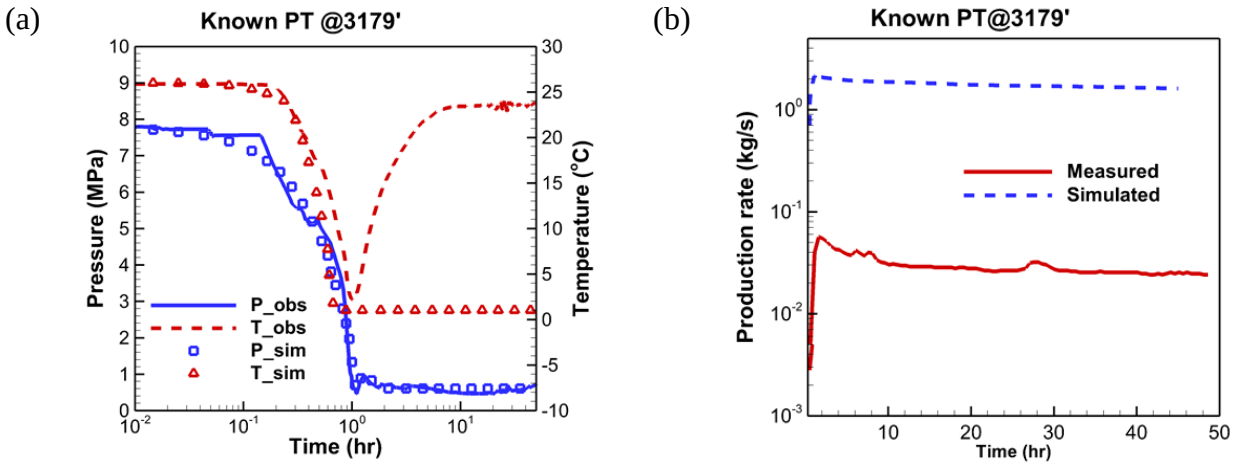

Figure 7. Results for P-T held constant at the well top shown by (a) pressure and temperature variation over time during the production test as observed in the field experiment (lines) and in the model (symbols) at the lower gauge at depth = 3,180 ft (969.26 m) 1 ft from the well top with permeability as shown in Table 1, and by (b) measured and simulated mass production rate at the top of the well and at 968.96 m, respectively.

To try to improve upon the agreement between simulation and observations, we lowered the permeability of the feed zones Resv1 and Resv3 by a factor of ~200 to 0.4136×10^{-18} m^2 and 20.04×10^{-18} m^2, respectively. The idea was to try to mimic effects of hypothesized hydrate that could be plugging up the pores of the near-well region and lowering effective permeability. For these lower-permeability conditions, the pressure match as shown in Figure 8 is good and the temperature follows the correct qualitative trend, but it does not fall initially as much and it recovers faster compared to the observations in the field experiment. This is indicative of a shorter period of decompression cooling occurring in the simulation than in the experiment, which could arise by a dearth of CO_2 available for decompression and phase change.

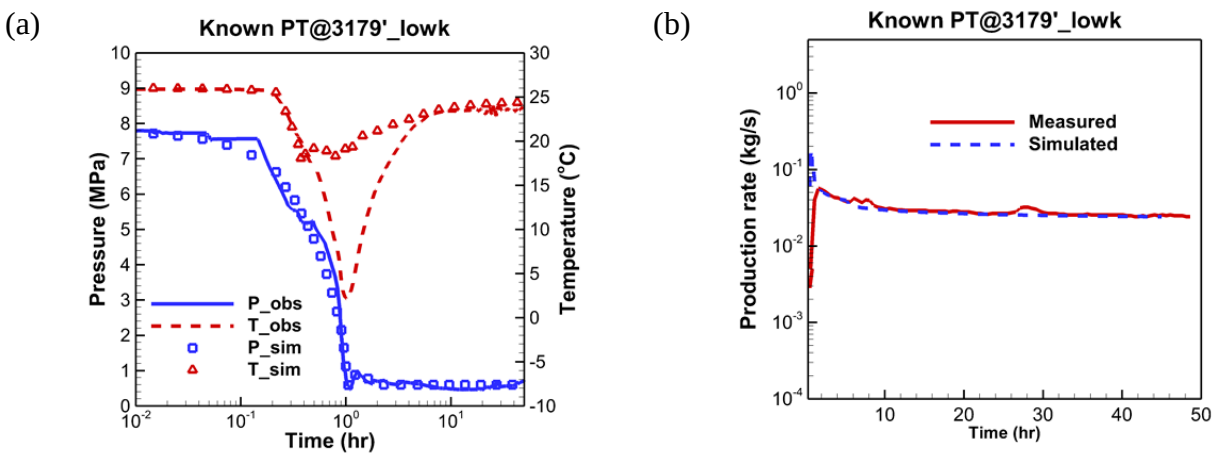

Figure 8. Results for P-T held constant at the well top shown by (a) pressure and temperature variation over time during the production test as observed in the field experiment (lines) and in the model (symbols) at the lower gauge at depth = 3,180 ft (969.26 m) 1 ft from the well top with reduced permeability in the feed zones, and by (b) measured and simulated mass production rate at the top of the well and at 968.96 m, respectively.

Building upon the observation that low permeability of the reservoir was helping to produce a better match to temperature observations, but that not enough cooling was occurring early on and recovery was too quick, we concluded that the system was behaving as if there was a larger volume of easily accessed CO_2 that could decompress early in the experiment, but limitations in CO_2 supply later in the experiment. One way to conceptualize this is to assume the near-well region has higher permeability than the regions farther away from the well. While this hypothesized high-permeability region around the well was not independently measured or confirmed, several processes related to well completion likely created such a zone. In particular, there is first the drilling of the well that can creates a narrow damage zone consisting of small microfractures around the boring. Second and much more important is the perforating of the well by the use of shaped charges that vaporize and rubblize rock as they burst through the casing into the formation. Finally, the well was acidized at high pressure, further enhancing permeability in the near-well region. A sketch of the hypothesized configuration is shown in Figure 9. This permeability structure allows fluid near the well to flow out of the well early in the test, but still restricts the flow later in the test as CO_2 is sourced farther from the well in the low-*k* far-field regions.

The values we used for the radially varying permeability field are shown in Table 3. As shown in Figure 10, the simulation using this radially varying permeability field can match the *P-T* evolution and the long-term mass production rate. What is happening in this model is that CO_2 from the wellbore and in the near-well region is relatively easily produced early in the test and its expansion and vaporization serve to severely lower the BH temperature. But the available volume of CO_2 easily accessed is limited, and later in the test the low-*k* of the reservoir severely

limits CO_2 flow and the temperature rises as heat from the formation flows to the cold well and raises the temperature. We note that other processes such as hydrate formation during the production test could give rise to an early high-permeability and late low-permeability configuration that could possibly mimic the near-well high-permeability and far-field low-permeability system tested here. But regardless of the cause of restricted flow of CO_2, the fact is that without some interventions such as well stimulation or hydrate inhibition, the Danielson 33-17 well would not produce CO_2 at the rates needed for the proposed BSCSP project.

Table 3. Radial permeability variation used to simulate production test data.

Rock	k (R < 0.522 m) (10^{-18} m^2)	k (R > 0.522 m) (10^{-18} m^2)
Resv1	84.4	0.1712
Resv3	4090.0	8.296

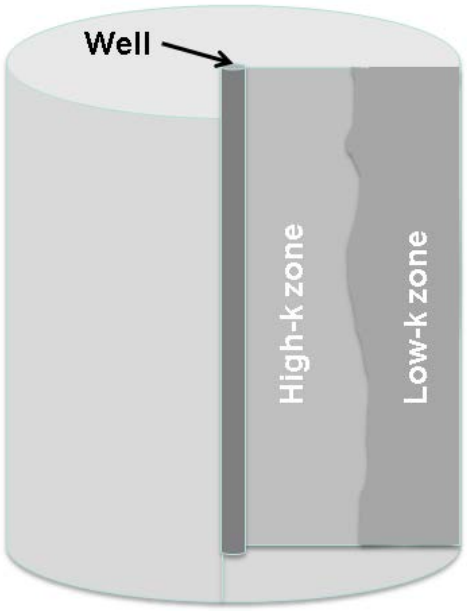

Figure 9. Schematic of high-k region of thickness 0.522 m around the well that allow a good match between simulation and observation of the Danielson 33-17 production test results.

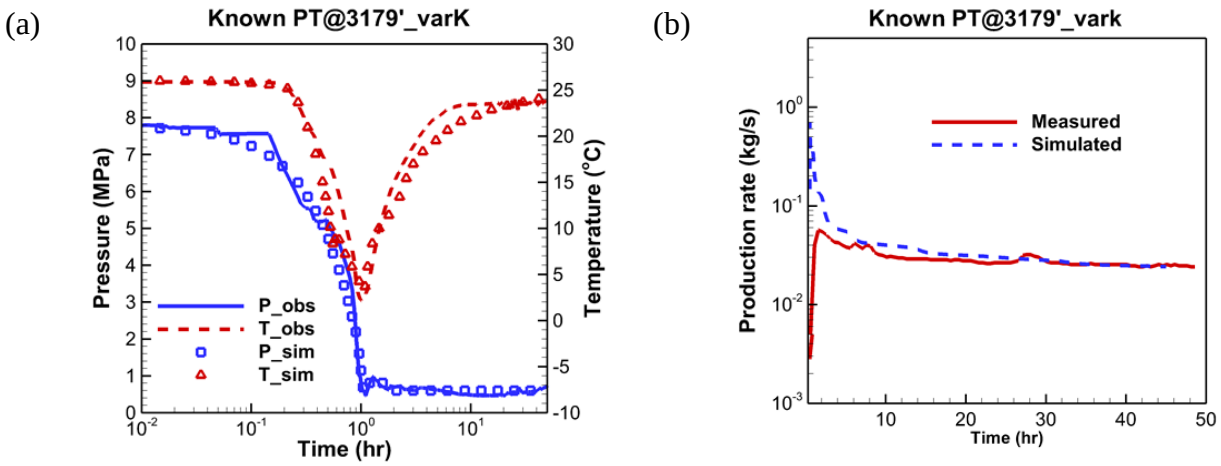

Figure 10. Results for P-T held constant at the well top with radially varying permeability as shown by (a) pressure and temperature variation over time during the production test as observed in the field experiment (lines) and in the model (symbols) at the lower gauge at depth = 3,180 ft (969.26 m) 1 ft from the well top with radially varying permeability field as shown in Table 3, and by (b) measured and simulated mass production rate at the top of the well and at 968.96 m, respectively. Note that the flow rate data were not reliably measured during the first couple of hours of the test due to a problem with the orifice plate that was solved later).

Parameter study of CO_2 production

Putting aside the details of the 2014 Danielson 33-17 production test and considering instead the problem of the production or withdrawal of CO_2 from subsurface reservoirs in general, we present here results of a parameter study laying out conditions of reservoir depth and transmissivity for which CO_2 extraction is expected to be feasible and conditions under which production/withdrawal may require special mitigations against low permeability and/or hydrate formation.

The prototypical reservoir we consider is assumed to be at near-hydrostatic pressure at the each given depth (e.g., 10 MPa at 1010 m) and with a typical geothermal gradient (27.5 ^{o}C/km and 15 ^{o}C at surface). The initial CO_2 saturation in the reservoir is 80% while the aqueous phase saturation is set to 20% which is below the residual saturation (aqueous phase is immobile). A constant pressure-support boundary condition 1 km away from the well center is maintained during production. The reservoir is fully perforated with a 7-inch production casing connected to 4-inch tubing up to the wellhead. The transmissivity (permeability-thickness product) of the reservoir varies from 2×10^{-15} to 2×10^{-11} m^3 and the depth of the reservoir varies from 910 to 1,510 m (Table 4). In all cases, a constant wellhead pressure of 4 MPa is enforced during 1,000 hours of production to give a constant production condition to compare the reservoir performance and the average production rate is calculated as an indicator of productivity (except for two cases of 2×10^{-14} m^3 transmissivity at depths of 1,410 m and 1,510 m for which the

simulation ended earlier (250 and 517 hours, respectively) due to too much water accumulating at the well bottom. The wellbore is discretized as a 1D column connected to the reservoir which comprises a 1D radial grid extending out to a radius of 1 km.

Table 4 Parameter variations in sensitivity study

Parameters	Transmissivity (permeability-thickness product) m^3	Depth (m)
Values	2×10^{-15}, 2×10^{-14}, 2×10^{-13}, 2×10^{-12}, and 2×10^{-11}	910, 1010, 1110, 1210, 1310, 1410, and 1510

The simulations are performed using research versions of T2Well[23,24] and ECO2M[19] that solve for three-phase flow and have several improvements for enhancing convergence when liquid-gas phase change occurs. The heat exchange between flowing well and surrounding cap rock is calculated using a semi-analytical equation for heat flow. The tubing wall, casing annulus, and other well assembly parts are approximated to be part of the surrounding cap rock with the heat conductivity of 2.51 W/m ^oC. The same heat conductivity is used for the reservoir rocks.

The results of 35 runs (five transmissivity levels and seven depths) of the parameter study (Table 4) are shown in Figure 11 as a contour plot of production rate (kg/s) as a function of reservoir depth on the *Y*-axis and transmissivity on the *X*-axis. In general, the deeper the reservoir the higher the pressure and temperature will be leading to significantly higher production rate for the given production pressure (specified at the wellhead). However, the transmissivity of the reservoir becomes the dominant factor in controlling the production rate for smaller transmissivities. As the transmissivity decreases to below 1000 md-m (= 3.0 on the X-axis on Figure 11), the production rate drops with the reservoir transmissivity while the rate only slightly increases with reservoir depth. Such nonlinear behavior as a result of combined effects of the reservoir depth and transmissivity reflects the influence of CO_2 as a highly compressible fluid on the production rate under various conditions which would not be expected to be seen in the case of incompressible fluids such as water (not shown here). In all cases, there are small amounts of liquid water produced although the water saturation in the reservoir (0.2) is below the residual aqueous phase saturation (0.3), indicating aqueous phase formed during flow up the well by condensation.

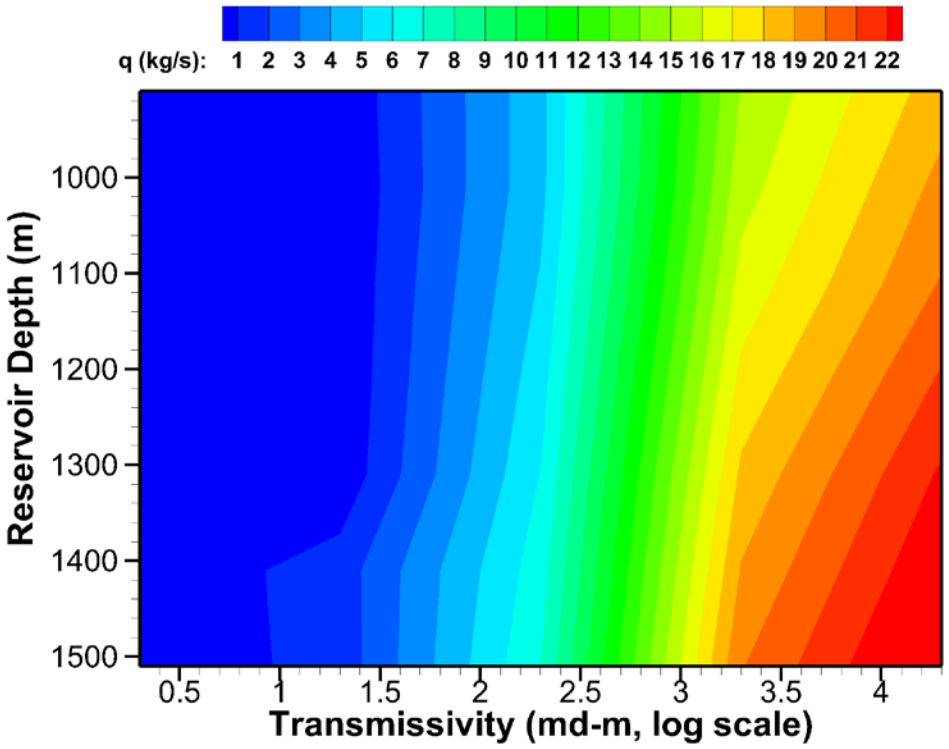

Figure 11. Average total mass production rate (over 1,000 hours of production) under constant wellhead pressure of 4 MPa as a function of reservoir depth and transmissivity (thickness × permeability).

The pressure and temperature drop significantly as the fluid flows from the reservoir to the well bottom as shown in Figure 12. Such drops are mainly the result of expansion cooling. For the deeper reservoir cases (higher *P*-*T*), the drop in well-bottom pressure increases monotonically with the decrease of the transmissivity. However, for the cases with shallower reservoir (lower *P*-*T*), the drop in well-bottom pressure is not monotonically related to the transmissivity. This is because of complicated phase-change and phase-interference behavior of CO_2 in the well within the particular *P*-*T* ranges occurring in the well.

(a)

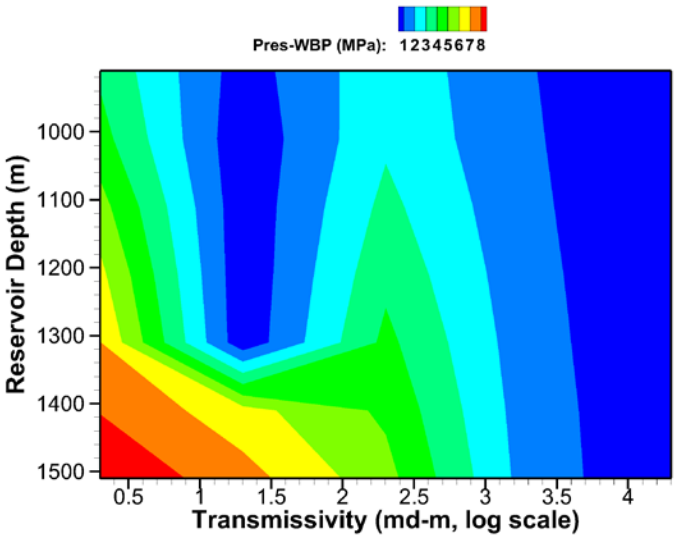

(b)

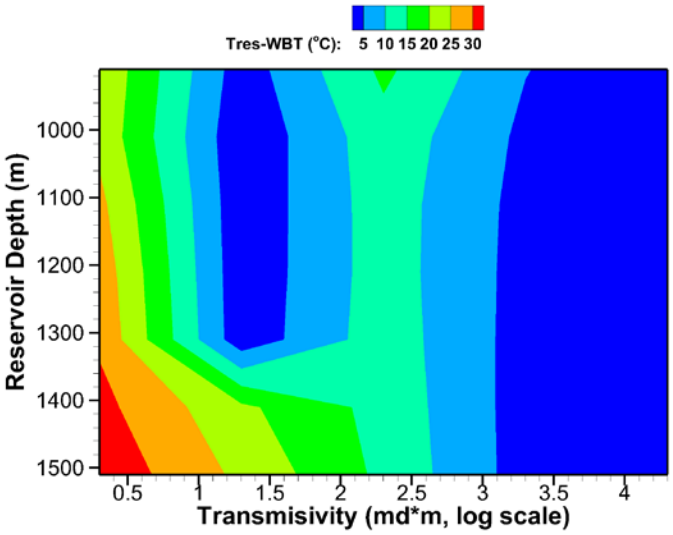

Figure 12. (a) Contours of pressure drop and (b) temperature drop at the well bottom as a function of reservoir depth and transmissivity at the end of 1,000 hours of production.

In order to explain the well-bottom pressure and well-bottom temperature results shown in Figure 12, we show in Figure 13 profiles of saturation, pressure, and temperature along the well for the particular case of a reservoir at a depth of 910 m as an example. As shown, the gas saturation for transmissivity of 2×10^{-14} m^3 (= 1.3 on the *X*-axis of Fig.12) is much lower than for other cases (either lower or higher transmissivity), resulting in higher well-bottom pressure because of larger gravity force due to the denser liquid CO_2 in the well. For the cases with higher transmissivity, the CO_2 usually converts from supercritical to two- (gas- and liquid- CO_2) phase conditions on the way up to the wellhead with relatively higher gas saturation (~0.8). Because of relatively higher flow rate, the temperature profile is controlled mostly by expansion cooling. As a result, both pressure and temperature decrease almost linearly with elevation because of gradual change in phase saturations as well as the average density of the fluids. On the other

hand, in the case of very small transmissivity (2×10^{-15} m^3, = 0.3 on the *X*-axis of Fig. 12), the CO_2 almost instantly converts into gaseous CO_2 from its supercritical state at the well bottom. Because the flow rate is very small, the cold CO_2 gas can be easily heated by the surrounding formation so the temperature quickly recovers from the lowest point at the well bottom and the temperature profile becomes very close to the ambient geothermal profile above the depth of 600 m.

The case with transmissivity of 2×10^{-14} m^3 is a special case for which the balance between the inflow enthalpy and the wellbore-formation heat exchange results in larger liquid saturation (~0.8) than the other cases in the two-phase CO_2 section of the well. As a result, the pressure quickly increases with depth below the all-gas region near the top to almost overlap the profile of the case with the highest transmissivity (2×10^{-11} m^3) until the end of the two-phase CO_2 region. The lowest temperature occurs at shallow depth where the two-phase CO_2 ends and all liquid CO_2 evaporates to form a gas phase, which is different from the cases of either higher transmissivity (lowest *T* at wellhead) or lower transmissivity (lowest *T* at the well bottom).

(a)

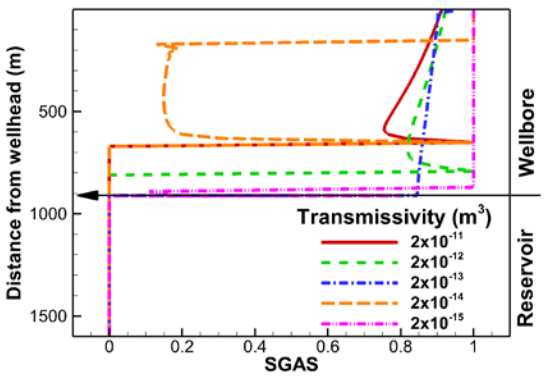

(b)

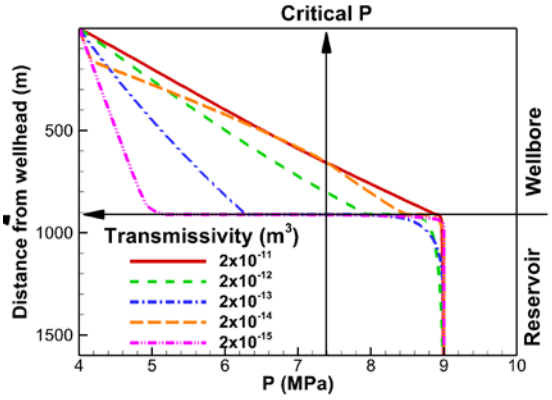

(c)

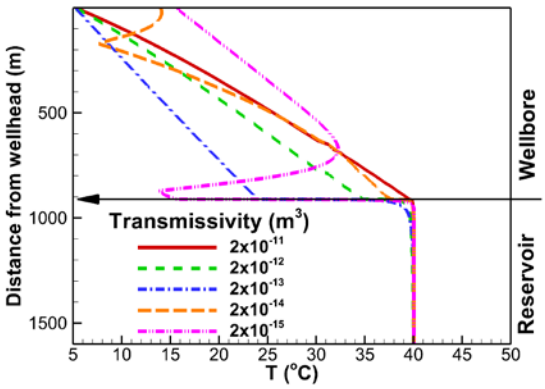

Figure 13. Profiles of (a) gas-CO_2 saturation, (b) pressure, and (c) temperature after 1,000 hours of production at constant production pressure (4 MPa) for the cases of a reservoir at a depth of 910 m with various transmissivities.

Discussion and Conclusions

The 2014 CO_2 production test from Kevin Dome, Montana showed very low temperatures occurring at the well bottom and also very low overall fluid and CO_2 production rate. The low ambient (pre-test) temperature of the reservoir means that CO_2 liquid is stable at the depth of the middle Duperow where the test was conducted. Our simulations show that CO_2 liquid flowing from the reservoir into the well during the production test likely flashed to vapor. Severe cooling

accompanies this phase change, while further expansion-related cooling of the gas during the production test serves to reduce well-bottom temperature even more. The low temperatures recorded (~2 ºC) suggest that hydrates and/or water ice could form to limit CO_2 production. By hypothesizing a relatively high-permeability damage zone along the well with a lower-permeability region outboard of the damage zone, we could match the simulation results to the observations for pressure, temperature, and long-term flow rate. It appears that the effect of the high-permeability region is to provide an initial mass of CO_2 to be relatively easily produced resulting in expansion and phase-change-related cooling, while the low-permeability region slows down flow to the well and allows temperature recovery by thermal conduction through the formation rock. Although the near-well relatively high-permeability region could be due to damage during drilling, perforating, or acidizing, the observed production and *P-T* data may also be controlled by the formation of hydrate or ice during the production test which could result in an initial high-permeability system transitioning to a low-permeability system roughly mimicking the near-well damage zone hypothesis. Another effect of severe cooling could be geomechanical, as thermal stresses would tend to cause the rock to contract and potentially increase permeability as fractures open. We have taken the approach of Occam's Razor and attempted to explain observations by the simplest model possible rather than invoking hydrate, ice, or thermal fracture creation. Regardless of the details of what causes permeability variation in the near-well region, our simulations show that producing CO_2 from cold and low-permeability reservoirs is very challenging and may require engineered solutions such as well stimulation and/or bottom-hole heaters to improve productivity.

To address the question of CO_2 production more generally, we carried out a parameter study to determine the dependence of flow rate on reservoir depth and transmissivity. We found that large transmissivity and greater depth favor CO_2 production, and that the flow rate varies non-linearly with transmissivity and depth over the range we investigated. The profiles of saturation, pressure, and temperature in the well column show strong sensitivity to transmissivity. In general, our simulation results for Kevin Dome and for CO_2 reservoirs in general may be a useful starting point for operators interested in evaluating production potential and/or for engineering solutions for enhancing production, especially from cold and low-permeability CO_2 reservoirs.

Acknowledgment

We thank four anonymous reviewers for constructive comments that improved the presentation of this study. This material is based upon work supported by the U. S. Department of Energy and the National Energy Technology Laboratory under Award Number DE-FC26-05NT42587. Additional support was provided by Lawrence Berkeley National Laboratory under Department of Energy Contract No. DE-AC02-05CH11231. This report was prepared as an account of work sponsored by an agency of the United States Government. Neither the United States Government nor any agency thereof, nor any of their employees, makes any warranty, express or implied, or

assumes any legal liability or responsibility for the accuracy, completeness, or usefulness of any information, apparatus, product, or process disclosed, or represents that its use would not infringe privately owned rights. Reference herein to any specific commercial product, process, or service by trade name, trademark, manufacturer, or otherwise does not necessarily constitute or imply its endorsement, recommendation, or favoring by the United States Government or any agency thereof. The views and opinions of authors expressed herein do not necessarily state or reflect those of the United States Government or any agency thereof.

References

1. Oldenburg, C.M., 2016. How the low price of oil can spur CCS research innovation. Greenhouse Gases: Science and Technology, 6(1), pp.1-2.
2. Allis, R., Chidsey, T., Gwynn, W., Morgan, C., White, S., Adams, M. and Moore, J., 2001, May. Natural CO_2 reservoirs on the Colorado Plateau and southern Rocky Mountains: Candidates for CO_2 sequestration. In Proceedings of the First National Conference on Carbon Sequestration (pp. 14-17). US Department of Energy, National Energy Technology Laboratory Washington, DC.
3. Zhou, Z., Ballentine, C.J., Schoell, M. and Stevens, S.H., 2012. Identifying and quantifying natural CO_2 sequestration processes over geological timescales: The Jackson Dome CO_2 Deposit, USA. Geochimica et cosmochimica acta, 86, pp.257-275.
4. Muro, H.G., Campos, S.B., Cancino, L.O.A. and José, A., 2007. Quebrache, a Natural CO_2 Reservoir: A new source for EOR projects in Mexico. Paper SPE, 107445.
5. Gachuz-Muro, H., Sanchez Bujanos, J.L., Castro Herrera, I. and Rodriguez Pimentel, J.A., 2011, January. Quebrache Field: Evaluations to Date of this Natural CO2 Reservoir. In SPE EUROPEC/EAGE Annual Conference and Exhibition. Society of Petroleum Engineers.
6. Oldenburg, C.M., Joule-Thomson cooling due to CO_2 injection into natural gas reservoirs, Energy Conversion and Management, 48, 1808-1815, 2007. LBNL-60158.
7. Ziabakhsh-Ganji, Z. and Kooi, H., 2014. Sensitivity of Joule–Thomson cooling to impure CO_2 injection in depleted gas reservoirs. Applied Energy, 113, pp.434-451.
8. Oldenburg, Curtis M., Migration mechanisms and potential impacts of CO_2 leakage and seepage, in Wilson and Gerard, editors, Carbon Capture and Sequestration Integrating Technology, Monitoring, and Regulation, pp 127-146, Blackwell Publishing, 2007. LBNL-58872.
9. Brock, W.R. and Bryan, L.A., 1989, January. Summary results of CO_2 EOR field tests, 1972-1987. In Low permeability reservoirs symposium. Society of Petroleum Engineers.
10. Kuuskraa, V.A., Godec, M.L. and Dipietro, P., 2013. CO_2 utilization from “next generation” CO_2 enhanced oil recovery technology. Energy Procedia, 37, pp.6854-6866.
11. Renfro, J.J., 1979. Sheep Mountain CO_2 production facilities-a conceptual design. *Journal of Petroleum Technology*, *31*(11), pp.1-462.
12. Lynch, R.D., McBride, E.J., Perkins, T.K. and Wiley, M.E., 1985. Dynamic kill of an uncontrolled CO2 well. journal of Petroleum Technology, 37(07), pp.1-267.

13. Weeter, R.F. and Halstead, L.N., 1982. Production of CO_2 from a reservoir-a new concept. *Journal of Petroleum Technology*, *34*(09), pp.2-144.
14. Jokhio, S.A., Tiab, D. and Escobar, F.H., 2001, January. Quantitative analysis of deliverability, decline curve, and pressure tests in CO2 rich reservoirs. In SPE Permian Basin Oil and Gas Recovery Conference. Society of Petroleum Engineers.
15. BSCSP, Big Sky Carbon Sequestration Partnership, 2012. http://www.bigskyCO_2.org/about/rcsp.
16. Dai, Z., Stauffer, P.H., Carey, J.W., Middleton, R.S., Lu, Z., Jacobs, J.F., Hnottavange-Telleen, K. and Spangler, L.H., 2014. Pre-site characterization risk analysis for commercial-scale carbon sequestration. Environmental science & technology, 48(7), pp.3908-3915.
17. Onishi, T., M.C. Nguyen, J.W. Carey, R. Will, W. Zaluski, D.W. Bowen, B.C. Devault, A. Duguid, Q. Zhou, S.H. Fairweather, L.H. Spangler, P.H. Stauffer, 2018. Potential CO_2 and brine leakage through wellbore pathways for geologic CO_2 sequestration using the National Risk Assessment Partnership tools: Application to the Big Sky Regional Partnership. International Journal of Greenhouse Gas Control (submitted).
18. Pan, L., Spycher, N., Doughty, C. and Pruess, K., 2015. ECO2N V2. 0: A TOUGH2 fluid property module for mixtures of water, NaCl, and CO_2. Scientific report LBNL-6930E.
19. Pruess, K., 2011. ECO_2M: a TOUGH2 fluid property module for mixtures of water, NaCl, and CO_2, including super-and sub-critical conditions, and phase change between liquid and gaseous CO_2.
20. Jung, Y., Pau, G.S.H., Finsterle, S. and Pollyea, R.M., 2017. TOUGH3: A new efficient version of the TOUGH suite of multiphase flow and transport simulators. Computers & Geosciences, 108, pp.2-7.
21. Van Genuchten, M.T., 1980. A closed-form equation for predicting the hydraulic conductivity of unsaturated soils 1. Soil science society of America journal, 44(5), pp.892-898.
22. Corey, A.T., 1954. The interrelation between gas and oil relative permeabilities. Producers monthly, 19(1), pp.38-41.
23. Pan, L., C.M. Oldenburg, Y.-S. Wu, and K. Pruess, Transient CO2 leakage and injection in wellbore-reservoir systems for geologic carbon sequestration, Greenhouse Gases: Sci. and Tech., 1(4), 335-350, 2011. LBNL-5248E.
24. Pan, L., and C.M. Oldenburg. "T2Well—An integrated wellbore–reservoir simulator." Computers & Geosciences 65 (2014), 46-55.